Gold-Diaphragm Based Fabry-Perot Ultrasonic Sensor for Partial Discharge Detection and Localization

Wei Zhang,[1] Ping Lu ,[1] *Senior Member, IEEE*, Wenjun Ni,[2] Wanze Xiong,[1] Deming Liu,[1] and Jiangshan Zhang[3]

[1]National Engineering Laboratory for Next Generation Internet Access System, School of Optical and Electronic Information, Huazhong University of Science and Technology, Wuhan 430074, China
[2]School of Electrical and Electronic Engineering, Nanyang Technological University, Singapore 639798, Singapore
[3]Department of Electronics and Information Engineering, Huazhong University of Science and Technology, Wuhan 430074, China

DOI:10.1109/JPHOT.2020.2982460

Manuscript received December 17, 2019; revised March 9, 2020; accepted March 17, 2020. Date of publication March 23, 2020; date of current version May 26, 2020. This work was supported in part by the National Natural Science Foundation of China under Grant 61775070 and in part by the Fundamental Research Funds for the Central Universities under Grants 2019kfyXMBZ052 and 2017KFYXJJ032. Corresponding author: Ping Lu (e-mail: pluriver@mail.hust.edu.cn).

Abstract: Acoustic measurement is the most widely used non-electric method to detect partial discharge (PD) signals by detect the ultrasonic waves arisen from partial discharge. To solve the shortages of low sensitivity and susceptibility to interferences, a gold diaphragm based Fabry-Perot interferometer ultrasonic sensor is proposed and experimentally demonstrated. Its high acoustic sensitivity and directional insensitivity shows great capability for PD detection and localization. Experimental results illustrate a well acoustic response from 20 kHz to 150 kHz when standard ultrasonic signals applied. The frequency range covers the acoustic frequencies derived from PD process. The ultrasonic signals from a discharge source is measured by the proposed fiber optic sensor with difference distances and incident angles. The output shows an attenuation of 1.32 dB/m and the sensor can detect weak signals as far as 3 m. The directional deviation coefficients are less than 10% for each measuring distance which exhibits directional independence. Two localization techniques with a sensor array (four sensors) are proposed and simulations are carried out to verify them feasible. The fiber-optic ultrasonic sensor may have a great potential in stability maintenance of electrical power systems due to its low cost, compact structure, environmentally robustness and simple manufacturing.

Index Terms: Fiber-optic sensors, fabry-Perot, ultrasonic detection, partial discharge.

1. Introduction

High voltage equipment play a significant role in the stability of any electrical power system. Partial discharge (PD) is worth attention in routine inspection. It's generated in a small area such as insulating bubble and internal air gap. Also, the discharge energy is too small to influent the short-term insulation strength. However, long-term discharge can cause regional insulation failure and further, breakdown. Besides, active gases such as ozone and nitric oxide generated by long-term discharge can corrode the insulation structure under the role of heat and then cause

thermal breakdown. So PD detection and localization have become an important testing method in the inspection and maintenance work of power grid as a precautionary measure [4].

Accompanied by PD process, there are also ionization, thermal radiation, acoustic emission, photon emission and other physical phenomena. According to these phenomena, there arises numerous methods to detect PD signals. The pulse capacitive coupler method is recommended by IEC60270 for its high sensitivity and quantitative analysis ability. However, its detection frequency band is overlapped with the severe electromagnetic interference band at site which has a strong impact on its sensitivity and signal-to-noise ratio (SNR). Ultra-high frequency (UHF) detection method realizes a shift on its detection frequency over 300 MHz to resist the interference, therefore it can be utilized interiorly for online monitoring. But the measuring process is complicated and some changes to the structure of the electrical power system are necessary to make before online monitoring. Other methods such as electrochemical gas detection method, nanometer gas sensing method and optical detection method are limited by cross interferences caused by pressure and temperature, equivalence between optical and electrical signals and technical immaturity, though they all show advantages of anti-interference of electromagnetic.

It is well-known that weak ultrasonic signals from 20 kHz to 300 kHz are generally emitted as soon as PD occurs. The poor performance of traditional ultrasonic detection method such as piezoelectric transducer (PZT) acoustic sensor consists in huge electromagnetic interferences generated by power appliance [5]. Under such a circumstance, fiber-optic ultrasonic sensor shows its superiority of compact size, immune to electromagnetic interferences, internal testing capability and resistance to chemical corrosion. Moreover, it has favorable characteristics of long life, fast response and high accuracy [6]. So fiber-optic ultrasonic sensors have great potentials in the field such as power transformers and gas insulated switchgear (GIS) system for PD monitoring, as well as discharge source localization.

There are many kinds of fiber-optic ultrasonic that have been researched in recent years, including fiber Bragg grating (FBG) based sensor [7], [8], fiber laser based interferometric sensor [9], [10], Sagnac interferometric sensor [11], [12], and diaphragm based Fabry-Perot interferometric sensor [13], [14] and taper based sensor [15], [16]. Among the fore-mentioned ultrasonic sensors, some are applied in the PD detection. A fiber-optic Michelson interferometric sensor for ultrasonic detection in electrical power system has been proposed [17]. The sensitivity for acoustic detection is 1.7 rad/(m·Pa) and the detectable frequency reaches to 150 kHz. The sensor head shows great feasibility and practicability when utilized at the distance of 10 cm. It may have a potential application for PD online monitoring of high-voltage cable accessories in power system. A FBG based PD sensor is designed to measure PD generated in a transformer via Bragg wavelength shifts detected by a spectrum analyzer [18]. A Sagnac interferometric sensor is designed for PD detection in power cables. The amplitude of PD signals in time-domain varies from 0.8 V to 1.9 V when applied voltage set to be 10 kV and the detectable frequency is up to 58 kHz [19]. A MEMS-based fiber-optic extrinsic Fabry-Perot ultrasonic sensor demonstrates the performance of its PD detection at different distances and different incident angles. There exists a 5.9 dB amplitude fluctuation when incident angle within the $\pm 60^{\circ}$ limitation The sensor also exhibits an exciting ability to detect weak PD signals as far as 3 m away due to its high SNR [20]. In the above-mentioned works, PD signals are acquired by fiber-optic sensors as a novel way, but some of them are cost unfriendly and implementation complex or can just detect outside the power system which faces the problem of signal attenuation.

In this paper, a gold diaphragm based Fabry-Perot interferometric ultrasonic sensor for PD detection is proposed. Its sensing performance of the standard ultrasonic signals is firstly examined and the acoustic response from 20 kHz to 150 kHz is investigated. It shows great result that the acoustic response range covers the frequencies derived from partial discharges. Afterwards, the directionality and distance sensitivity of the sensor are tested. The results show that it is sensitive enough to detect a weak signal as far as 3 m. Besides, the signal fluctuations with different incident orientations are small enough as that the sensor features directional insensitivity, which means, it is allowed to locate the PD source in space with a sensor array. Amplitude ratio localization technique and Time Difference of Arrival (TDOA) localization technique based on a sensor array with four

sensors are proposed and simulated to be feasible at the end of this paper. The proposed fiber-optic ultrasonic sensor applies ultra-thin diaphragm in partial discharge detection which greatly improves its sensitivity. The compact size allows the sensor to work inside high-voltage power equipment and the low cost significantly improves economic efficiency. Moreover, the localization techniques without electrical methods reduce the complexity of the detection process.

2. Principle

The main component of the ultrasonic sensor is the optical diaphragm. When the ultrasonic wave acts on the diaphragm, the diaphragm will deform. The deformation on the diaphragm varies from radial positions. When the diaphragm deformation is less than 30% of its thickness, it is considered to be small disturbance bending and the deformation can be approximately described as [1]:

$$d(r) = \frac{3\left(1-\mu^2\right)}{16Eh^3}\left(r^2-R^2\right)^2 p \tag{1}$$

where μ and E are Poisson's ratio and Young's modulus of the diaphragm material respectively, h and R are the thickness and radius of the diaphragm, respectively. Besides, r refers to the distance from the particle to the center of the diaphragm, p indicates the applied static pressure. The static pressure sensitivity of the diaphragm is expressed as the ratio of its deformation and the applied acoustic pressure. In this work, it can be approximately taken as the fiber aligned with the center of the diaphragm. The static pressure sensitivity can be expressed as below ($r = 0$):

$$S = \frac{d(0)}{p} = \frac{3\left(1-\mu^2\right)}{16Eh^3}R^4 \tag{2}$$

In order to promote the sensitivity, the radius and thickness of diaphragm need to be optimized. Moreover, it can be realized by selecting materials with more appropriate Poisson's ratio and Young's modulus. However, the acoustic pressure sensitivity of the diaphragm is not only determined by its static pressure sensitivity, but also the acoustic frequency. The dynamic pressure sensitivity of the diaphragm can be further described as:

$$S_a = \frac{3\left(1-\mu^2\right)R^4}{16Eh^3}\frac{f_{mn}^2}{\sqrt{\left(f_{mn}^2-f_a^2\right)^2+2f_a^2\frac{\xi}{\rho h}}} \tag{3}$$

where ρ and ξ are respectively the density of the diaphragm material and the damping coefficient of the diaphragm forced vibration. f_a refers to the acoustic frequency, f_{mn} is the resonant frequency of mn order mode, which can be described as:

$$f_{mn} = \frac{k_{mn}^2}{4\pi R^2}\sqrt{\frac{E}{3\rho\left(1-\mu^2\right)}} \tag{4}$$

where k_{mn} is a constant coefficient depending on the mn order mode. The fundamental resonant frequency f_{00} can arrive at a certain value when $m = n = 0$ under which circumstance k_{00} is equal to 3.196. It's easily deduced from the expression above that the dynamic pressure sensitivity of the diaphragm is not flat along the frequency range but peaking at the resonant frequency of the diaphragm. Considering the frequency band of the ultrasonic deriving from PD, the resonant frequency of the diaphragm should keep far below the range from 20 kHz to 150 kHz. So the characteristics selection of the diaphragm material is of crucial importance. The diameter of diaphragm is designed to be large in order to promote its sensitivity, but also, the size of proposed sensor should be compact to make it convenient in application. Some properties of the common materials are shown in Table 1.

In this work, gold is selected to be the diaphragm material. Compared with the silicon film and graphene diaphragm in the previous work [3], it features smaller Young's modulus and bigger Poisson's ratio to ensure its high sensitivity. With the addition of size design of the sensing probe, the resonant frequency is located much lower. The gold diaphragm is designed to be 300 nm in

TABLE 1
Some Properties of Several Common Materials

Material	Poisson's ratio μ	Young's modulus E (GPa)	Density ρ(kg/m^3)
Silica	0.17	73.7	2200
Silicon	0.3	170	2350
Graphene	0.16	1000	2200
Gold	0.42	79.5	19300
Polymer	0.3	2~8	850~1350
Aluminum	0.35	69	2700

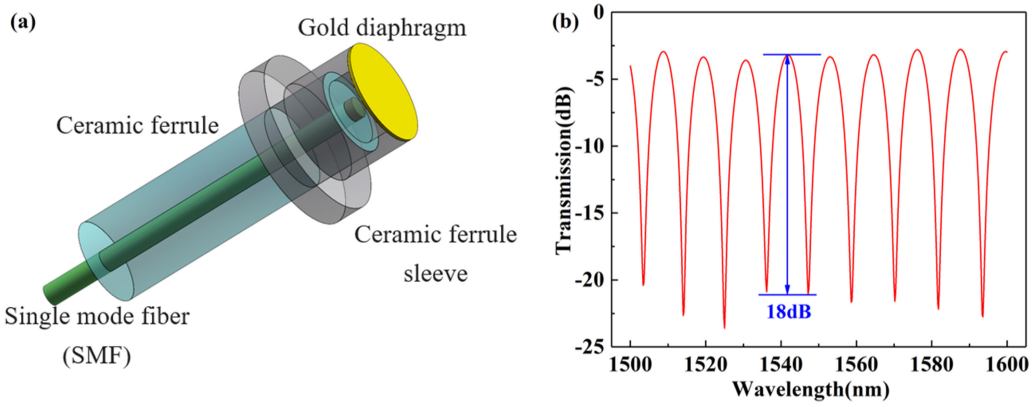

Fig. 1. (a) The structure design sketch of the proposed sensor and (b) Spectrum.

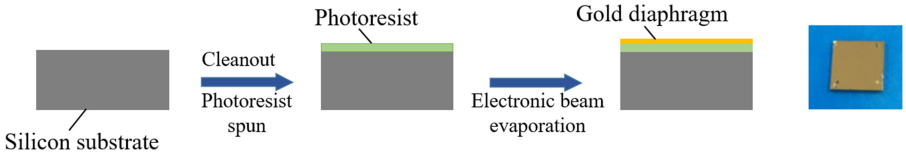

Fig. 2. The preparation process of the schematic diagram of the gold diaphragm.

thickness and 2.5 mm in diameter. According to the characteristics of gold diaphragm, the pressure sensitivity is calculated to be 278.51 nm/kPa at 40 kHz.

3. Sensor Fabrication

The structure of the ultrasonic sensor is depicted in Fig. 1(a). A section of single mode fiber (SMF) is inserted into the inner ceramic ferrule whose inner diameter is 125 μm. The size of proposed sensor should be compact to make it convenient, but the diameter of diaphragm The inner ceramic ferrule is then inserted into the well matched outer ceramic ferrule with the inner diameter of 2.5 mm. It is noteworthy that the outer ceramic ferrule is side opened to ensure the pressure equilibrium between the Fabry-Perot cavity and the external environment. A metal sleeve with the inner diameter of 3.2 mm is utilized to immobilize the whole structure.

The gold diaphragm is prepared as follows and shown in Fig. 2: The monocrystalline silicon with the size of 8 $\times$ 8 mm, thickness of 0.5 mm is chosen as the substrate. Firstly, it is polished and washed by acetone solution and ethanol in an ultrasonic cleaner. The residual solution is removed

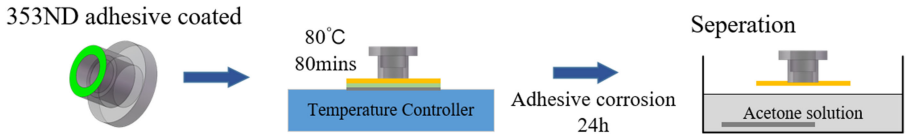

Fig. 3. The transfer process of the schematic diagram of the gold diaphragm.

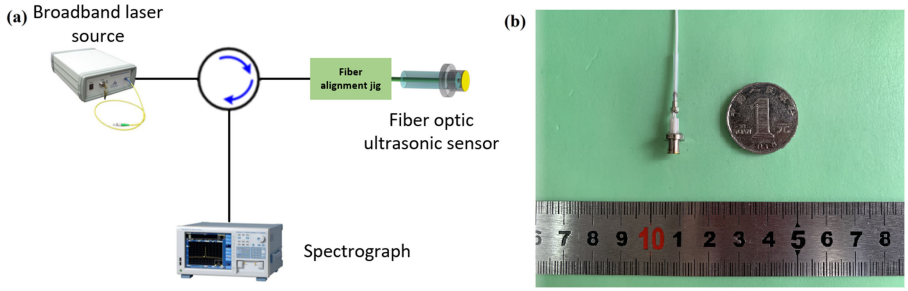

Fig. 4. (a) Diagram of cavity adjustment system. (b) Photograph of the fiber-optic ultrasonic sensor.

by deionized water. Secondly, after dried, the silicon is placed on a spin coater to spin photoresist (AZ5214) on it. For the convenience to remove the photoresist subsequently, the rotate speed of the spin coater needs lowering to increase the thickness of the photoresist to several microns. The rotate speed is set to be 800 r/min. The photoresist needs to be solidified by heating under the temperature of 60 °C for 1 min. Finally, the gold diaphragm is coated on the silicon substrate on a coating machine by electronic beam evaporation. The thickness is set to be 300 nm. The extremely thin diaphragm can greatly promote the sensitivity of the ultrasonic sensor. Because of the low rotate speed of the spin coater, the thickness of photoresist is not uniform which results in the unsmooth corners of the gold diaphragm. It is of little influence because diameter of the sensor probe in this paper is only 2.5 mm.

After prepared, the gold sample should be transferred to the surface of ceramic ferrule sleeve as the procedure shown in Fig. 3. Firstly, the component A and B of the epoxy resin adhesive (353ND) are mixed up with the mass proportion of 10:1 after which the mixture is coated on the surface of the sleeve. Then the sleeve is nipped by a tweezer and falls vertically on the gold sample. 80 minutes are taken for the adhesive curing under the temperature of 80 °C, after which the gold sample together with the sleeve is immersed in the analytical acetone solution with the concentration of 99.99%. Under the corrosion condition for 24 hours, the photoresist is thoroughly moved away, thus the gold diaphragm is transferred from the silicon substrate to the surface of the sleeve. The probe is moved transversely off the substrate and then slightly lifted away from the solution lest the diaphragm be damaged by surface tension of liquid. Finally, it is kept quiescent for 1 hour to ensure the acetone totally volatilized since which the gold diaphragm is successfully transferred. Depression of the diaphragm doesn't appear compared to the graphene diaphragm in the previous work [3]. Thus, the performance of the sensor is further promoted.

The FP cavity is equivalent to the length between fiber end-face and gold diaphragm. Fig. 4(a) shows the cavity adjustment system. The cavity length is adjusted with the help of an alignment jig and a horizontal platform. At the same time, the reflected light of the FP interference is exhibited on a spectrometer (AQ6370C-20, YOKOGAWA). When the contrast of the interference spectrum reaches its peak value, the sensor head and its tail fiber are fixed together with the AB adhesive. The spectrum is shown in Fig. 1(b). The contrast and the free spectrum range (FSR) are respectively about 18 dB and 12 nm.

After fabricated, the photograph of the fiber-optic ultrasonic sensor is shown in Fig. 4(b). The maximum diameter of the sensor is only 5 mm and the length of the whole sensor is less than

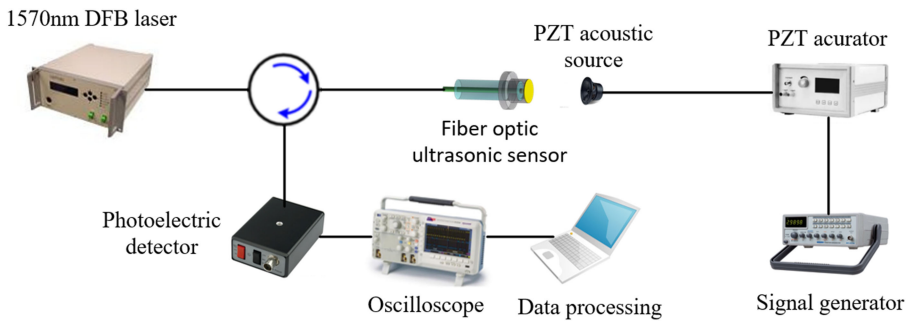

Fig. 5. Diagram of the proposed PD and ultrasonic sensing system.

2.5 cm. The transferred diaphragm looks smooth and robust compared with that in the previous work. The structure is very compact compared to other types of ultrasonic sensors.

4. Results and Discussion

4.1 Experiment Setup

The structure of ultrasonic sensing system for partial discharge detection is demonstrated in Fig. 5. The tuned monochromatic light whose wavelength corresponds to the quadrature point is launched into an optical circulator and then propagates into the ultrasonic sensing probe. Two reflected lights respectively from fiber end face and deformable diaphragm generate interference light which transmits backwards and is therewith detected by a photoelectric detector (PD, New Focus 1623) via the same optical circulator. Converted electrical signal is then presented on an oscilloscope (DPO2012, Tektronix) and subsequently processed by computer. The ultrasonic wave as the kind of mechanical wave deforms the diaphragm periodically at the sound frequency to modulate the interference light. Afterwards ultrasonic with the information of PD signals can be demodulated by data processing. A high-voltage power supply is utilized to actuate the discharge model in the air.

To verify the ability of the proposed optic-fiber ultrasonic sensor to detect PD signals, its performance of known standard ultrasonic signals is firstly demonstrated. The standard ultrasonic signals are generated by the PZT which is actuated by a piezoelectric ceramic actuator (E1200, COREMORROW). A signal generator (33250A, Agilent) sends signals with specific frequency and amplitude to the actuator.

4.2 Standard Ultrasonic Signals Experiment

During the experiment process, the sensor is kept away from both the acoustic source with the distance of 2 cm. The detected acoustic frequencies of standard signals covering the band from 20 kHz to 150 kHz are generated with the step of 10 kHz and the amplitude is kept 10 V. The results are showed below.

As is shown in Fig. 6(a), (b), the signals with the frequency of 60 kHz and 110 kHz are listed as illustrations. The V_{pp} of the ultrasonic signals detected by the proposed optic-fiber sensor are 0.42 V and 0.36 V respectively. The weakening of the detected signals of higher frequencies may be ascribed to the increasing attenuation coefficient of ultrasonic signals with frequency augmentation in the air. The time domain waveforms obtained can reach a conclusion that the ultrasonic waves are perfectly detected without any distortion. Then, a Fast Fourier Transform (FFT) is performed with the purpose of frequency response investigation and SNR determination of the entire detection system. The obtained signals correspond greatly with the standard signals generated by the ultrasonic transducer. The two frequencies have the similar SNRs of 44 dB and 48 dB respectively. Further, the acoustic response is investigated as shown in Fig. 7.

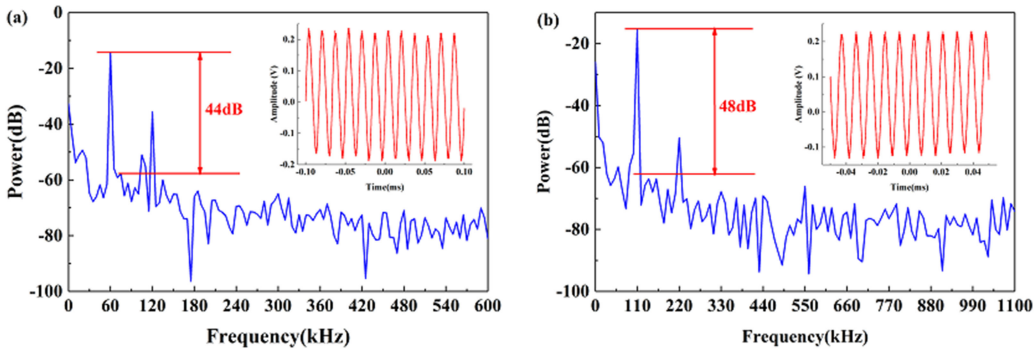

Fig. 6. Two known standard ultrasonic signals detected by the proposed sensor. The single frequency experimental results are (a) 60 kHz and (b) 110 kHz, respectively.

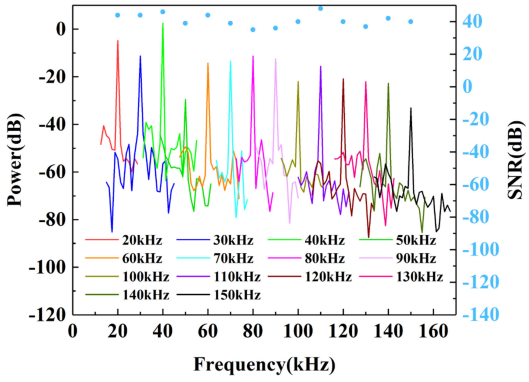

Fig. 7. The acoustic response of the proposed sensor.

Within the frequency band from 20 kHz to 150 kHz, the frequency of 80 kHz has the minimal SNR of 35 dB. On the other hand, the frequency of 110 kHz has the maximal SNR of 48 dB. Because the frequency band is far away from the resonant frequency and taken experimental randomness into consideration, the frequency band from 20 kHz to 150 kHz can be well detected which allows a better performance for the sensor to detect PD signals.

4.3 Discharge Detection Experiment

The discharge detection is examined as the same way. During the experiment process, the sensor is kept away from discharge source with the distance of 2 cm. Fig. 8(a) shows the diagram of discharge sensing system. The discharge model powered by a high voltage power supply is utilized to generate discharges in the air. In one discharge pulse, the signal amplitude comes to the peak instantaneously and attenuate continuously as shown in Fig. 8(b). It is defined that V_{pp} equals to the peak amplitude of the detected signal. Because of the randomness of each pulse, the peak amplitudes fluctuate in a small range on the same condition. So at least 10 discharge pulses are measured and the averaged V_{pp} value provides the accuracy in the entire experiment.

For different distances, a distance sensitivity can be given out as the ratio of the detected V_{pp} and distance. As a demonstration, the ultrasonic signals of discharges when the distances set as 25, 100, 175cm are shown in Fig. 9(a), (b), (c) shows the detected signals in the time domain. The pulse separation is about 50 ms, that is, the pulse frequency is about 20 Hz. And the pulse duration is about 40 ms. The pulse signals can be apparently distinguished from the background noise even at the distance of 175 cm for that the signal is as great as 10 times as the noise. In this sensing system, the leading component of noise is from laser source which shows slight

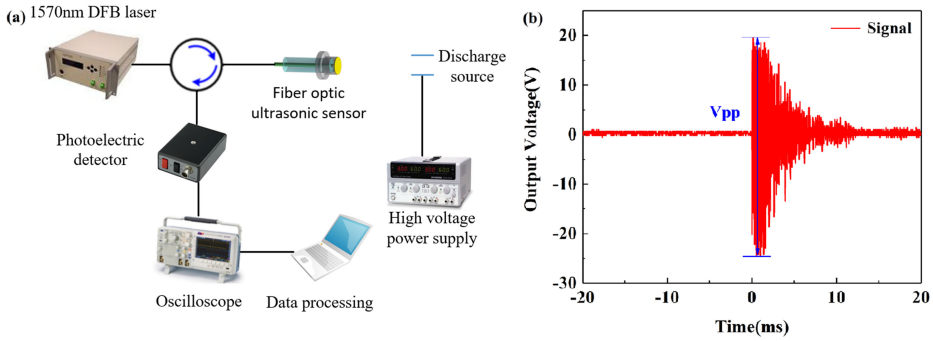

Fig. 8. (a) Diagram of the discharge sensing system. (b) The detected mono-pulse ultrasonic signal.

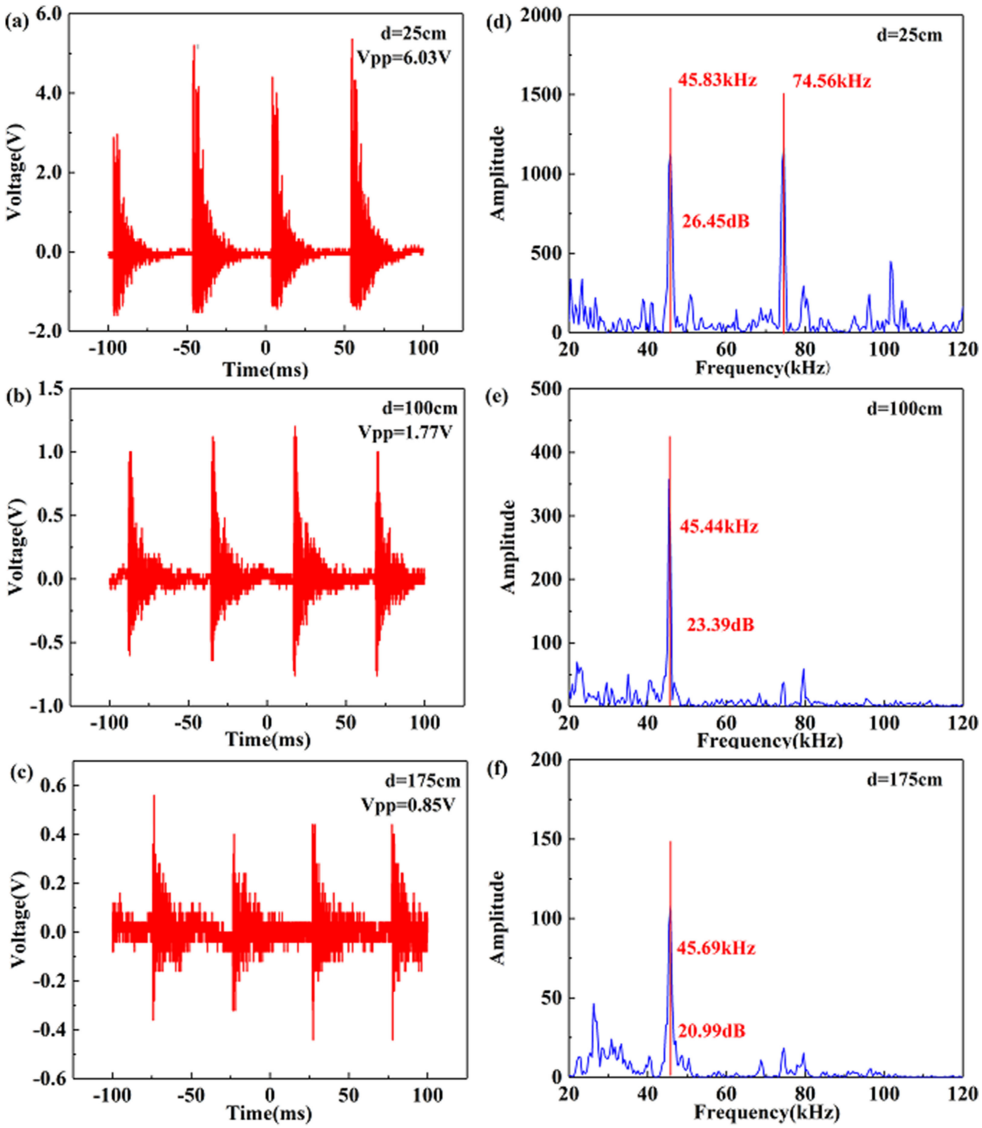

Fig. 9. The detected ultrasonic signals from discharges at the distance of 25, 100, and 175 cm in (a), (b), and (c) the time domain; (b), (e), and (f) the frequency domain.

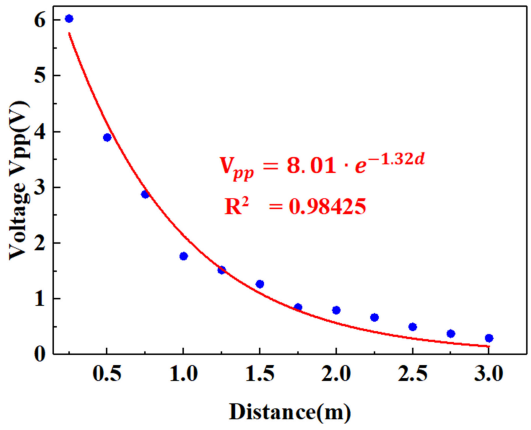

Fig. 10. The detected ultrasonic signals at different distances.

instability at long-time operation. After FFT in OriginPro, the frequency domain information is shown in Fig. 9(d), (e), (f). It shows that all the detected signals are centered on the frequency components of 45.83 kHz. Another frequency peak of 74.56 kHz can be observed at the distance of 25 cm. The SNR is also calculated for each distance. It gives out as 31.52 dB, 23.37 dB and 20.53 dB at the distance of 25, 100, 175 cm respectively

Fig. 10 shows the different V_{pp} values at the different distances varying from 25 cm to 300 cm with a step of 25 cm. It is presented to be an exponential decay relationship between the detected V_{pp} and distances. After the exponential fitting in OriginPro, the expression is given out as:

$$V_{pp} = 8.01 e^{-1.32d} \tag{5}$$

Which is corresponding to the decaying property of ultrasonic waves in the air. By evaluating the logarithm of V_{pp} values, a linear relationship is given out as:

$$V_e = \ln \frac{V_{pp}}{V_0} = 2.08 - 1.32d \quad (dB) \tag{6}$$

in which V_0 is the reference value. Based on the analysis above, the distance sensitivity S_d is worked out as -1.32 dB/m. Equation (5) and (6) are only suitable for the situation when the distance between discharge source and ultrasonic sensor is large than 0.25 m. When the distance is too small, the error will be relatively large.

Besides the distance sensitivity, the directional property of the ultrasonic sensor is also worth researching. In the process of the experiment, the sensor head is rotated to ensure different ultrasonic incident angles. The angle step is set to be 15° in the range from 0° to 360°. At each angle, different incident distances are set to be 50, 100, 150, 200 cm to investigate the directional property more comprehensively. As shown in Fig. 11(a), the directional responses at each distances are really flat. Defining the ratio of standard deviation and the mean value as deviation coefficient. They are calculated to be 4.37%, 7.67%, 9.3% and 7.65% at each distances respectively. Thus the ultrasonic sensor can be regarded as directionally independent. It is a great characteristic for PD detection and localization because of its weak-signals recognition ability for all directions.

4.4 Localization Technique Simulations

The output voltage of the sensor is not only determined by the distance from discharge source, but also related to the discharge intensity which influences the ultrasonic acoustic pressure. In this work, it is not able to detect specific discharge quantity so far, but by means of comparing

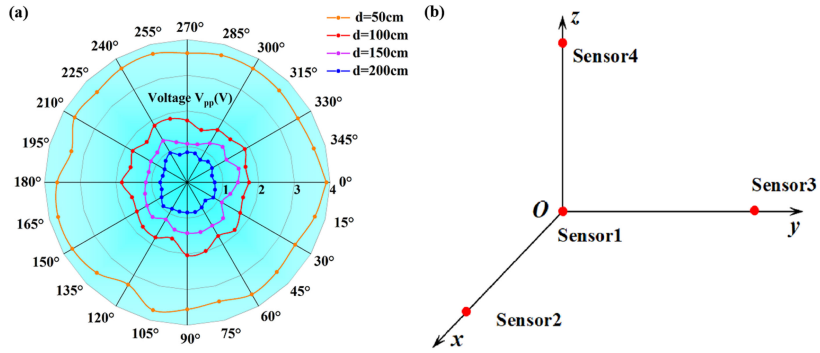

Fig. 11. (a) The directional property at different distances and (b) the coordinate of sensor array.

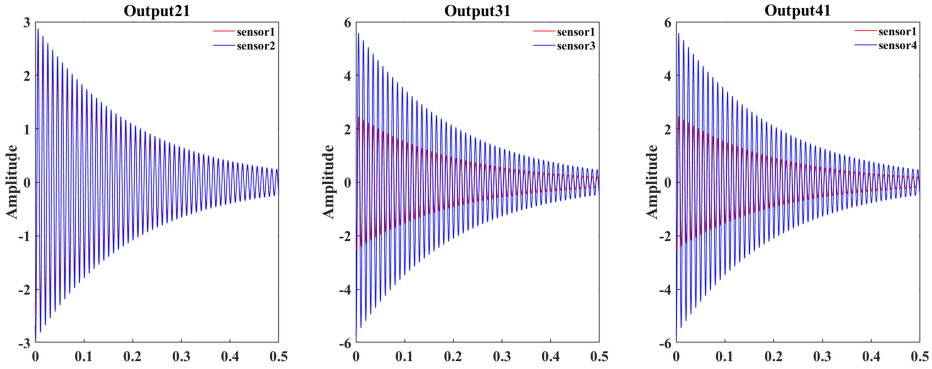

Fig. 12. The directional property at different distances.

different outputs from different sensors, the discharge source can be located. Theoretical analysis and simulation are demonstrated.

Considering the different discharge intensity, the output voltage $V\prime pp$ can be expressed as:

$$V'_{pp} = 8.01Ae^{-1.32d} \tag{7}$$

in which A is a constant relevant to the discharge intensity. Four sensors are arranged in an array and labelled numerical number shown in Fig. 11b. It is worth noting that the sensors can't be put in a same plane. For a simplex discharge source, different sensors will obtain different outputs. Compare any two outputs of the sensors, it is easy to reach the following expression:

$$\ln\frac{V_{oj}}{V_{oi}} = -1.32\left(d_j - d_i\right) \quad i, j = 1, 2, 3, 4 \tag{8}$$

where V_{oj} and V_{oi} are the $V\prime pp$ of the j th and the i th sensor, respectively. d_j and d_i are the distance from the j th sensor and the i th sensor to the discharge source. The coordinate of the discharge source can be calculated from the equation set.

To verify the localization technique proposed, a MATLAB simulation is carried out. The coordinates of four sensors are set to be (0, 0, 0), (1, 0, 0), (0, 1, 0) and (0, 0, 1) in meters, respectively. The signal model is set to be the product of a sinusoidal signal and a decaying exponential signal When the coordinate of the discharge source set to be (1, 3, 3) in meters, the detected signals of sensor2, sensor3, sensor4 compared to sensor1 are shown in Fig. 12. The output ratios of each sensor to sensor1 are 1.1166, 2.2639 and 2.2639, respectively. And the coordinate of discharge source is calculated to be (1.0105, 3.0547, 3.0547) in meters, which is close to the setting

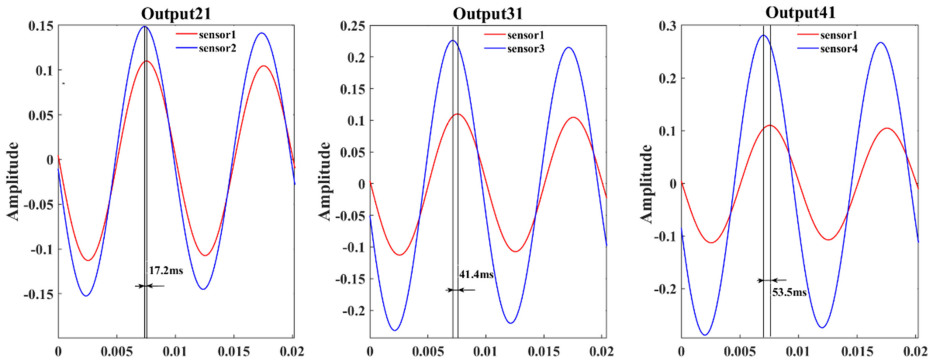

Fig. 13. The directional property at different distances.

coordinate. Thus the amplitude ratio localization technique is capable of locating the discharge source.

Another localization technique based on TDOA (Time Difference of Arrival) technique is proposed. It is called triangulation source localization technique for isotropic plates with known wave speed in [21] and three sensors are utilized and placed to form a triangle. In order to locate the discharge source in space. Four sensors are placed to form a pyramid to locate the discharge source in three dimensions. For a known insulting medium, the acoustic velocity can be seen as a constant. Similar to the ratio localization technique mentioned above, it is easy to reach the following expression:

$$c\left(t_j - t_i\right) = -1.32\left(d_j - d_i\right) \quad i, j = 1, 2, 3, 4 \tag{9}$$

where t_j and t_i are the acoustic travelling time from the source to the j th and i th sensor, respectively. d_j and d_i are the distance from the j th sensor and the i th sensor to the discharge source. c is the acoustic velocity in the insulting medium. The coordinate of the discharge source can be also calculated from the equation set.

To verify the TDOA localization technique, a MATLAB simulation is carried out in the same way. The coordinates of four sensors are set to be (0, 0, 0), (1, 0, 0), (0, 1, 0) and (0, 0, 1) in meters, to form a pyramid. When the coordinate of the discharge source set to be (2, 4, 5) in meters, the time difference of the detected signals of sensor2, sensor3, sensor4 compared to sensor1 are shown in Fig. 13. When c is set to be 1324 m/s, the time difference of arrival of sensor2, sensor3, sensor4 compared to sensor1 are 17.2 ms, 41.1 ms and 53.5 ms, respectively. The coordinate of the discharge source is calculated to be (2.0088, 4.0193, 5.0230) in meters, which is also close to the setting coordinate. So the TDOA localization technique is also able to locate the discharge source.

5. Conclusion

In conclusion, the directional insensitive fiber-optic ultrasonic sensor for PD detection is fabricated and experimentally demonstrated. The acoustic signals from 20 kHz to 150 kHz can be well detected with the high SNR up to 48 dB at 110 kHz. In discharge detection experiment, the sensor has the distance attenuation sensitivity of -1.32 dB/m and can well distinguish the signal and background noise as far as 3 m. The sensor shows insensitive to acoustic incident angle as the deviation coefficients are 4.37%, 7.67%, 9.3% and 7.65% at the distances of 50, 100, 150, 200 cm. Two simulations show the theoretical support for the proposed localization techniques and further test will be carried out to verify them. Moreover, quantitative measurement for PD detection will be studied. The fiber-optic ultrasonic sensor for PD detection may have a great potential in stability maintenance of electrical power systems.

References

[1] J. Deng, *Development of Novel Optical Fiber Interferometric Sensors With High Sensitivity for Acoustic Emission Detection: [Ph.D]*. Blacksburg, VA, USA: Virginia Polytechnic Institute and State University, 2004.

[2] W. Si, C. Fu, D. Li, H. Li, P. Yuan, and Y. Yu, "Directional sensitivity of a MEMS-based fiber-optic extrinsic Fabry–Perot ultrasonic sensor for partial discharge detection," *Sensors*, vol. 18, 2018, Art. no. 1975.

[3] N. Wenjun *et al.*, "Ultrathin graphene diaphragm-based extrinsic Fabry-Perot interferometer for ultra-wideband fiber optic acoustic sensing," *Opt. Express*, vol. 26, no. 16, pp. 20758–20767, 2018.

[4] M. M. Yaacob, M. A. Alsaedi, J. R. Rashed, A. M. Dakhil, and S. F. Atyah, "Review on partial discharge detection techniques related to high voltage power equipment using different sensors," *Photon. Sensors*, vol. 4, no. 4, pp. 325–337, 2014.

[5] W. Yu *et al.*, "Partial discharge ultrasound detection using the sagnac interferometer system," *Sensors*, vol. 18, no. 5, 2018, Art. no. E1425.

[6] Y. Li, P. Lu, C. Zhang, W. Ni, D. Liu, and J. Zhang, "Sensing characterization of helical long period fiber grating fabricated by a double-side CO_2 laser in single-mode fiber," *IEEE Photon. J.*, vol. 11, no. 3, Jun. 2019, Art no. 6801608.

[7] Q. Wu and Y. Okabe, "High-sensitivity ultrasonic phase-shifted fiber Bragg grating balanced sensing system," *Opt. Express*, vol. 20, pp. 27, 2012, Art. no. 28353.

[8] A. Rosenthal, D. Razansky, and V. Ntziachristos, "High-sensitivity compact ultrasonic detector based on a pi-phase-shifted fiber Bragg grating," *Opt. Lett.*, vol. 36, no. 10, pp. 1833–1835, 2011.

[9] T. Liu, L. Hu, and M. Han, "Adaptive ultrasonic sensor using a fiber ring laser with tandem fiber Bragg gratings," *Opt. Lett.*, vol. 39, no. 15, pp. 4462–4465, 2014.

[10] G. Liu, E. Sandfort, L. Hu, T. Liu, and M. Han, "Theoretical and experimental investigation of an intensity-demodulated fiber-ring-laser ultrasonic sensor system," *IEEE Sensors J.*, vol. 15, no. 5, pp. 2848–2855, May 2015.

[11] T. S. Jang, S. S. Lee, I. B. Kwon, W. J. Lee, and J. J. Lee, "Noncontact detection of ultrasonic waves using fiber optic Sagnac interferometer," *IEEE Trans. Ultrason. Ferroelect. Freq. Control*, vol. 49, no. 6, pp. 767–775, Jun. 2002.

[12] T. S. Jang, S. S. Lee, and Y. G. Kim, "Surface-bonded fiber optic Sagnac sensors for ultrasound detection," *Ultrasonics*, vol. 42, no. 1-9, pp. 837–841, 2004.

[13] P. C. Beard and T N Mills, "Extrinsic optical-fiber ultrasound sensor using a thin polymer film as a low-finesse Fabry-Perot interferometer," *Appl. Opt.*, vol. 35, no. 4, pp. 663–675, 1996.

[14] L. H. Chen *et al.*, "Miniature in vivo chitosan diaphragm-based fiber-optic ultrasound sensor," *IEEE J. Sel. Topics Quantum Electron.*, vol. 18, no. 3, pp. 1042–1049, May/Jun. 2012.

[15] Y. Li, X. Wang, and X Bao, "Sensitive acoustic vibration sensor using single-mode fiber tapers," *Appl. Opt.*, vol. 50, no. 13, pp. 1873–1878, 2011.

[16] R. G. Minasamudram *et al.*, "Thin film metal coated fiber optic hydrophone probe," *Appl. Opt.*, vol. 48, no. 31, pp. 77–82, 2009.

[17] Z. Tongzhi *et al.*, "A fiber-optic sensor for acoustic emission detection in a high voltage cable system," *Sensors*, vol. 16, no. 12, 2016, Art. no. 2026.

[18] B. Sarkar, C. Koley, N. K. Roy, and P. Kumbhakar, "Fiber Bragg grating sensor for on-line detection of partial discharge in high voltage power transformers," in *Proc. 12th Int. Conf. Fiber Opt. Photon., OSA Techn. Digest (online) (Opt. Soc. Amer.)*, 2014, Paper M3C.3.

[19] W. Yu *et al.*, "Partial discharge ultrasound detection using the sagnac interferometer system," *Sensors*, vol. 18, no. 5, 2018, Art. no. 1425.

[20] W. Si, C. Fu, D. Li, H. Li, P. Yuan, and Y. Yu, "Directional sensitivity of a MEMS-based fiber-optic extrinsic Fabry–Perot ultrasonic sensor for partial discharge detection," *Sensors*, vol. 18, 2018, Art. no. 1975.

[21] A. Tobias, "Acoustic-emission source location in two dimensions by an array of three sensors," *Non-Destructive Testing*, vol. 9, no. 1, pp. 9–12, 1976.